Biophysical Journal
Article

Biophysical Society

Dissecting the Forces that Dominate Dimerization of the Nucleotide Binding Domains of ABCB1

Dániel Szöllősi,[1] Gergely Szakács,[2] Peter Chiba,[3] and Thomas Stockner[1,*]
[1]Institute of Pharmacology, Center for Physiology and Pharmacology, [2]Institute of Cancer Research, and [3]Institute of Medical Chemistry, Center for Pathobiochemistry and Genetics, Medical University of Vienna, Vienna, Austria

ABSTRACT P-glycoprotein, also known as multidrug resistance protein 1 or ABCB1, can export a wide range of chemically unrelated compounds, including chemotherapeutic drugs. ABCB1 consists of two transmembrane domains that form the substrate binding and translocation domain, and of two cytoplasmic nucleotide binding domains (NBDs) that energize substrate transport by ATP binding and hydrolysis. ATP binding triggers dimerization of the NBDs, which switches the transporter from an inward facing to an outward facing transmembrane domain conformation. We performed MD simulations to study the dynamic behavior of the NBD dimer in the presence or absence of nucleotides. In the apo configuration, the NBDs were overall attractive to each other as shown in the potential of mean force profile, but the energy well was shallow and broad. In contrast, a sharp and deep energy minimum (∼−42 kJ/mol) was found in the presence of ATP, leading to a well-defined conformation. Motif interaction network analyses revealed that ATP stabilizes the NBD dimer by serving as the central hub for interdomain connections. Simulations showed that forces promoting dimerization are multilayered, dominated by electrostatic interactions between the nucleotide and conserved amino acids of the signature sequence and the Walker A motif. In addition, direct and water-bridged hydrogen bonds between NBDs provided conformation-defining interactions. Importantly, we characterized a largely unrecognized but essential contribution from hydrophobic interactions between the adenine moiety of the nucleotides and a hydrophobic surface of the X-loop to the stabilization of the nucleotide-bound NBD dimer. These hydrophobic interactions lead to a sharp energy minimum, thereby conformationally restricting the nucleotide-bound state.

INTRODUCTION

ABCB1 (also known as P-glycoprotein, P-gp, or MDR1) is a member of the ATP Binding Cassette (ABC) protein superfamily. ABCB1 is responsible for the multidrug resistance of cancer cells that leads to failure of chemotherapy treatment (1). The transmembrane domains (TMDs) recognize and translocate a wide variety of hydrophobic compounds (2). The conserved nucleotide binding domains (NBDs) bind and hydrolyze ATP, converting the chemical energy into conformational changes that lead to substrate translocation across the membrane.

The overall structure of ABCB1 shows a twofold pseudosymmetry with a TMD1-NBD1-linker-TMD2-NBD2 domain sequence. NBDs form dimers in a head-to-tail arrangement, while creating two composite nucleotide-binding sites (NBS) in their interface. The NBSs harbor a set of conserved motifs, including the A-loop (3), Walker A motif (4), Q-loop (5), X-loop (6), signature motif (7), Walker B motif (8), D-loop (9), and the H-loop (10) (see Fig. 1). Substrate translocation seems to follow an alternating access mechanism (11) implying a substrate binding site that is accessible exclusively from the intra- or the extracellular space. The substrate binding site is of high affinity in the inward facing state and of low affinity as the protein changes its conformation to an outward facing state (12). Unidirectionality of transport is imposed by coupling transport to ATP binding and hydrolysis. The exact mechanism of harvesting the energy stored in ATP, its conversion into conformational changes, and its directional substrate translocation remained enigmatic. ABCB1 shows basal ATPase activity that is uncoupled from substrate transport (13–15), whereas the presence of substrates increases the ATPase activity up to 10-fold (16). Several mechanistic models of the transport cycle have been proposed. These can be classified based on the predicted degree of NBD separation: the most important models include the tweezers-like (17) or the ATP switch model (18), which predict complete NBD separation, whereas the processive clamp (19), the alternating sites (14), or the constant contact model (20) suggest continuous NBD-NBD contact throughout the transport cycle. The

Submitted June 6, 2017, and accepted for publication November 14, 2017.
*Correspondence: thomas.stockner@meduniwien.ac.at
Editor: Chris Chipot.
https://doi.org/10.1016/j.bpj.2017.11.022

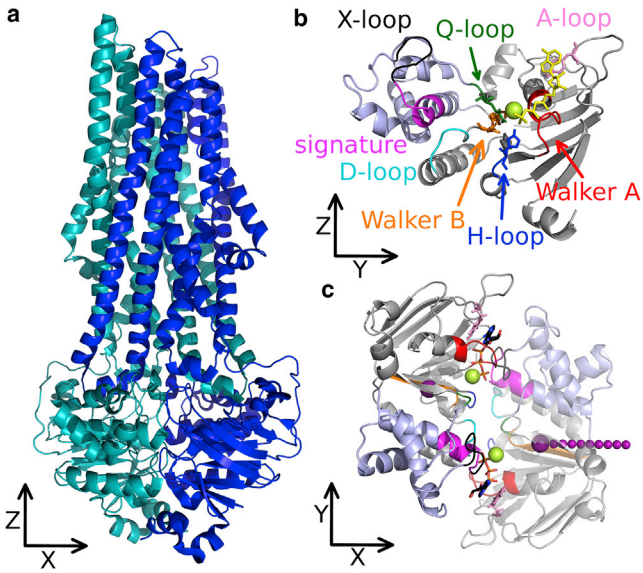

FIGURE 1 Structure and motifs of ABCB1. (*a*) Given here is a structural model of the full-length ABCB1 in the outward open state. (*b*) Interfacial view of the ABCB1 NBD with highlighted features: core subunit (*gray*), helical subunit (*light blue*), ATP (*yellow sticks*), Mg^{2+} (*light green*), and the NBD motifs. This color code is applied to all figures. The most important residue of each motif is highlighted in the same color as the motif: the tyrosine (Y401/Y1044) of the A-loop, the glutamine (Q475/Q1118) of the Q-loop, the histidine (H87/H1232) of the H-loop, the glutamine (Q530/Q1175) of the X-loop, and the glutamate (E556/E1201) of the Walker B loop are shown. (*c*) Given here is the simulation setup: cartoon representation of the NBDs of ABCB1 with bound ATP and Mg^{2+}. This conformation of the homology model is also at smallest center-of-mass distance. The center of mass of both domains is highlighted as a large purple sphere. The chain of smaller purple-colored spheres represents the center of mass of NBD2 of umbrella windows at increasing NBD separation used for the PMF calculations.

early models were based on biochemical evidence including ATPase and transport assays, mutational studies, chemical modification of cysteines, and nucleotide binding experiments. The crystal structures, showing widely separated NBDs, introduced the notion of extensive NBD separation during the transport cycle (21,22). Independent structural evidence for NBD motions came mainly from spectroscopic studies using EPR (23–25), FRET (26–28), and cysteine cross-linking (29–33). Not all data are fully consistent; therefore, the conformational changes of the transport cycle remained disputed. ABCB1 and homologs have been studied by simulations. Using unbiased or enhanced sampling methods, conformational transitions of the transport cycle (24,34–37), asymmetry (38–41), the effect of nucleotides on the overall transporter conformation (23,42–47), substrate translocation (42,48,49), and the influence of the environment on transporter stability (50) were investigated.

Despite the increasing amount of data, the exact mechanism of harvesting the energy stored in ATP, its conversion into conformational changes, and directional substrate translocation, remains unresolved. The aim of this study was to quantify the primary impact of nucleotides on NBD dimer conformation, interactions, and energy profiles. Unbiased MD simulations were combined with potential of mean force (PMF) calculations to reveal how these interactions shape the conformation of the NBD dimer, which leads to conversion of the chemical energy stored in ATP into mechanical forces that change the shape of the transporter and allow for directional substrate transport.

MATERIALS AND METHODS

The NBD of Sav1866 is 51 and 49% identical to NBD1 (residue 390–620) and NBD2 (residue 1033–1265) of ABCB1, respectively. The sequence alignment (51) is shown in Fig. S1. Models of the NBDs of ABCB1 were developed on the basis of Sav1866 (52) (PDB: 2ONJ). We used the software MODELLER, version 9.15 (53), to generate 50 models of ABCB1 based on the Sav1866 template applying the automodeling procedure of MODELLER and ranked the models by the DOPE score (54). The cocrystallized AMP-PNP served as template for ATP, whereas Na^{+} was replaced by Mg^{2+}. The best model according to the DOPE score was selected. The ADP-bound model of the NBDs of ABCB1 were created by removing the γ-phosphate moiety, whereas ATP and Mg^{2+} were removed to obtain the apo system. The binding mode of AMP-PNP is in good agreement with other crystal structures, in particular with the most recent mouse ABCB1 structure holding an ATP molecule in NBS1 (22). Within each NBS, we refer to the NBD that binds the nucleotide via A-loop and Walker A motifs as cis-NBD and the opposite NBD that interacts via its signature motif and the X-loop as trans-NBD. Structural details are shown in Fig. 1. Simulations were carried out using the AMBER99SB-ILDN force field (55). ATP and ADP parameters are based on the GAFF force field (56) and parameterization by Meagher et al. (57). Original parameters were converted to GROMACS format using ACPYPE (58).

All simulations were carried out with the software GROMACS, version 5.1 (59), using these homology models of the NBDs of ABCB1 (residues 390–620 and 1033–1265). All systems were solvated in water and 0.15 M NaCl and energy-minimized followed by a slow release protocol of stepwise reduction of position restraints (1000, 100, 10, and 1 $kJ*mol^{-1}*nm^{-2}$) on the Cα atoms, the two nucleotides, and the Mg^{2+} ions. Temperature was maintained at 310 K, applying velocity rescaling (60) and using 0.5 ps coupling time. Pressure was isotropically set to 1 bar with 20.1 ps coupling time using the Parrinello-Rahman barostat (61). A short-range cutoff of 0.9 nm was applied for electrostatic interactions, whereas long-range interactions were treated by the particle mesh Ewald method (62). Three systems for each configuration (apo, ATP, and ADP) were first independently equilibrated, followed by 400-ns-long unbiased simulations using a timestep of 2 fs.

We estimated the forces acting between the NBDs using PMF (63) calculations, applying umbrella sampling and the weighted histogram analysis method (64,65). The systems were initially oriented along their main axis and rotated so that the normal of the NBD-NBD interface is parallel to one main system axis. In the case of the ADP-bound configuration, we modified the side-chain rotamers of residue Q1118 and E1201 to obtain symmetric interaction with Mg^{2+} and nucleotide in both NBSs. Starting configurations were created by translating NBD2 (including the bound nucleotide and Mg^{2+} in NBS2) relative to NBD1 in 0.04 nm steps until 1.4 nm separation along an axis normal to the NBD-NBD interface. The generation of starting conformations was based on geometric considerations from crystal structures. The crystal structures of the eukaryotic ABCB1 transporters (mouse ABCB1; PDB: 4M1M (21) and *Caenorhabditis elegans* ABCB1; PDB: 4F4C (66)) showed that the NBDs separate along a path that is perpendicular to the NBD-NBD interface. We imposed symmetry in the movement of the NBDs to construct the reaction path of the PMF profile, because the crystal structures showed that the NBDs

also remained aligned at full separation (see Fig. S2). The transport cycle models, which predict full NBD separation (tweezers-like or the ATP switch model), frequently predict symmetric NBD movements. Additional windows were added between 0.12 and 0.48 nm NBD separation in 0.01 nm steps (see Fig. 1) to enhance sampling. Relative alignment of NBDs was maintained using the enforced rotation (ER) module (67), applied to both NBDs separately. Parameters of ER are set to remove the overall rotational and translational degree of freedom except the NBD center of mass distance along the reaction coordinate, by applying the pivot free radial motion method or the radial motion method to NBD2 and NBD1, respectively. The rotation force constant was set to 5000 kJ*mol^{-1}*nm^{-2}*deg^{-1}. Independence of the NBD-NBD center-of-mass motions from the applied ER restraints was estimated by correlating forces and torques. The analysis showed negligible correlation (0.2 at maximum).

The umbrella windows were simulated for 10 ns and increased to 20 ns at saddle points to obtain proper sampling. The distance of the Cα atoms of one NBD relative to the other NBD was restrained, including bound nucleotide and Mg^{2+}, if applicable. Assignment of the nucleotide to the selected NBD is based on experimental data (22,68–71), which show that nucleotide is bound to the A-loop and Walker A motifs. The applied harmonic force constant was set to k_{pull} = 5000 kJ*mol^{-1}*nm^{-2}. Upon improper sampling, the umbrella window was repeated by applying k_{pull} = 5000 kJ*mol^{-1}*nm^{-2} or k_{pull} = 25,000 kJ*mol^{-1}*nm^{-2}. Forces and center-of-mass distances were recorded every 20 ps. Convergence of the PMF curves was tested by the bootstrap method (64) applying 500 iterations. The potential energy of interaction among motifs, groups, molecules, and ions were calculated by quantifying the electrostatic and Lennard-Jones energy of interactions for the involved atoms, then summarized and averaged over the trajectories.

The ER module was applied to mimic the restraints that are imposed by the TMDs in the full transporter and would prevent free diffusion or free rotation of the NBDs, because TMDs and NBDs interact through the ICLs. This property of the architecture of full-length ABCB1 prevented us from directly evaluating the effect of the restraints as can be applied to fully independent proteins (72), because NBD1 and NBD2 are conformationally restrained by the TMDs and part of the same protein. Instead, to test the robustness of the reaction coordinate used in the PMF calculations, we continued each umbrella window simulation for 1 ns after removing the enforced rotation restraints. The distance between the NBDs along the axis of NBD-NBD separation was maintained using the same distance parameter (k_{pull} = 5000 kJ*mol^{-1}*nm^{-2}) as in the PMF calculations to prevent fast NBD-NBD association along the steep gradient of the reaction coordinate, which could hide other structural changes that evolve more slowly. Also, the NBDs rotate independently in free simulation, which leads to a misalignment between direction/axis of the distance restraints and the probed NBD dimer internal NBD-NBD distance. We therefore fixed in space the position of NBD1 using a force constant of 1000 kJ*mol^{-1}*nm^{-2}, whereas on NBD2 only the distance restraint along the axis of NBD-NBD separation was active. This setting allows uncovering potential higher energy conformation or additional gradients of rotation or translations of the relative NBD-NBD orientation, which were not probed for by the PMF calculation and could have been masked by the enforced rotation module. High energy conformation would therefore lead to a systematic deviation of showing a rotation or translation of NBD2 relative to NBD1.

RESULTS

We studied the NBDs of ABCB1 in the apo-, ADP-, and ATP-bound states using unbiased and PMF calculations. Overall rotations of the domains were removed in the biased simulations by the ER module (67), therefore allowing for improved sampling in the essential dimension of NBD separation. We could thereby probe for key interactions and investigate the role of specific contacts, while imposing a symmetric NBD separation, which is indicated by the NBD-NBD alignment observed in the crystal structures of mouse and *C. elegans* ABCB1 (Fig. S2) and implicitly or explicitly predicted by the transport models that include a state of full NBD separation (tweezers-like or the ATP switch model). The unbiased simulations complete the picture, highlighting motions and conformations. Substrate transport by ABCB1 is energized by ATP binding and hydrolysis. Simulations of the isolated NBD dimers allowed us to investigate ATP binding, NBD dimerization, and, importantly, to quantify the maximal primary/available energy generated by the NBDs, which can be harvested by ABCB1 for conformational changes resulting in substrate transport.

Interaction network

Analysis of the NBD dimer in the presence or absence of nucleotides revealed important interdomain interactions that depended on the type of bound nucleotide. We analyzed the final 200 ns of the unbiased trajectories, while treating the first 200 ns as additional equilibration. Within the equilibration phase, the conformation relaxed and converged to a conformational ensemble that was representative for the nucleotide setup. The representative final structure of each simulation is shown in Fig. S3. The interaction graphs (Fig. 2, *a–c*) quantified the cumulative analysis of interactions that were averaged over three independent simulations carried out for each configuration (apo, ADP, and ATP). Two motifs were considered to interact, if their average closest atom distance was <0.3 nm and therefore in direct contact. Fig. 2 highlights striking differences between the three configurations, as follows: 1) The apo simulations revealed mainly intradomain connections. Stable interactions between the two NBDs were observed between the Walker A motifs and the contralateral D-loop. NBS1 showed additional interdomain interactions, whereas NBS2 opened in all three simulations (as an example, see Fig. 2 *d*). 2) In the presence of ATP, simulations revealed a large and almost symmetric network of both intra- and interdomain interactions (Fig. 2 *b*). The two ATP molecules served as hubs for these interactions, mediating most interdomain connections. In addition, ATP binding also promoted new intradomain contacts. ATP therefore rigidified the NBD dimer, which is also reflected in the RMSD matrix (Fig. S4). The ATP-containing simulations showed only transient NBS openings, in contrast to the apo-and ADP-bound configurations. Structural parameters characterizing the overall conformation of each NBD (Fig. S5), the conformation of each NBS (Figs. S6 and S7), and the structural stability of bound nucleotides and Mg^{2+}, are given (Figs. S8 and S9). 3) The ADP-bound configuration showed in the independent simulations that NBS1 or NBS2 was less tightly packed. The representative structure closest to the mean (Fig. 2 *f*)

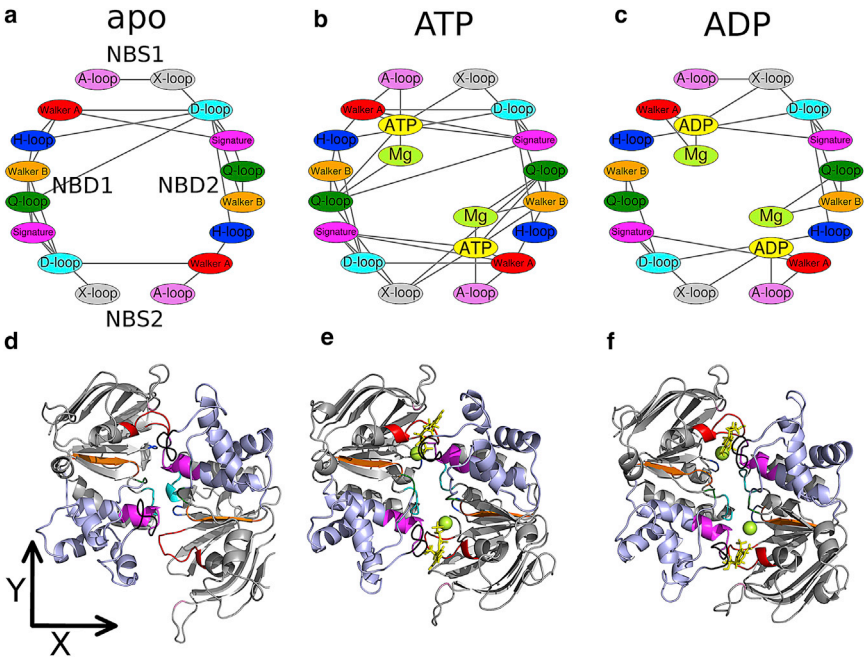

FIGURE 2 Motif interaction graph based on minimal distances for the apo-, ATP-, and ADP-bound NBD dimers. Connecting lines between motifs are drawn, if the minimal distance is <0.3 nm, averaged over the final 200 ns of the three independent simulations of the same system. Interaction graph of (*a*) the apo system, (*b*) the ATP-bound, and (*c*) the ADP-bound configurations. (*d–f*) Representative structures (closest to the mean structure of the final 200 ns) of apo-, ATP-, and ADP-containing simulations, respectively, with highlighted motifs (*colored* as in Fig. 1).

assumed an asymmetric conformation with the dissociation of the NBD2 core domain and the NBD1 signature motif resulting in opening of NBS2. Importantly, network analysis revealed a strong reduction of interdomain connections and a less symmetric pattern. Removal of the γ-phosphate significantly decreased the number of interactions. Interestingly, the Mg^{2+} ion assumed two mutually exclusive conformations: it was either bound to ADP or to the Walker B and Q-loop (Fig. S9). This is a clear difference to the presence of ATP, where both interactions can coexist.

Function of the phosphate groups

The phosphates of ATP and ADP interacted with both NBDs, most prominently with the Walker A (NBD1: residue 427–435; NBD2: residue 1070–1078) and signature motif (NBD1: residue 531–538; NBD2: residue 1176–1183). The interactions differed significantly between the two nucleotides in conformation, interaction pattern, and energies. We first analyzed the contribution of phosphate interactions to the potential energy, consisting of nonbonded electrostatic and van der Waals interactions, including hydrogen bonds (Fig. 3). The energetic analysis, averaging over the equilibrated second 200 ns of three trajectories, revealed that the α-phosphate (Pα + Oα) and the β-phosphate (Pβ + Oβ) have a dominant role in anchoring the nucleotide to the Walker A motif (ATP $= -497 \pm 97$ kJ/mol and ADP $= -504 \pm 111$ kJ/mol). Pα showed almost no interaction with the signature motif on the trans-NBD (Fig. 3, *a* and *b*, *blue* and *cyan*). Pβ strongly contributed to binding of ATP to the Walker A motif and therefore to the cis-NBD (Walker A-Pβ: ATP $= -325 \pm 99$ kJ/mol), while showing minimal interactions with the signature motif. In contrast, Pβ of ADP formed strong interactions with the signature motif (Pβ – signature motif: ATP $= -17 \pm 27$ kJ/mol and ADP $= -79 \pm 82$ kJ/mol). The strength of the interaction

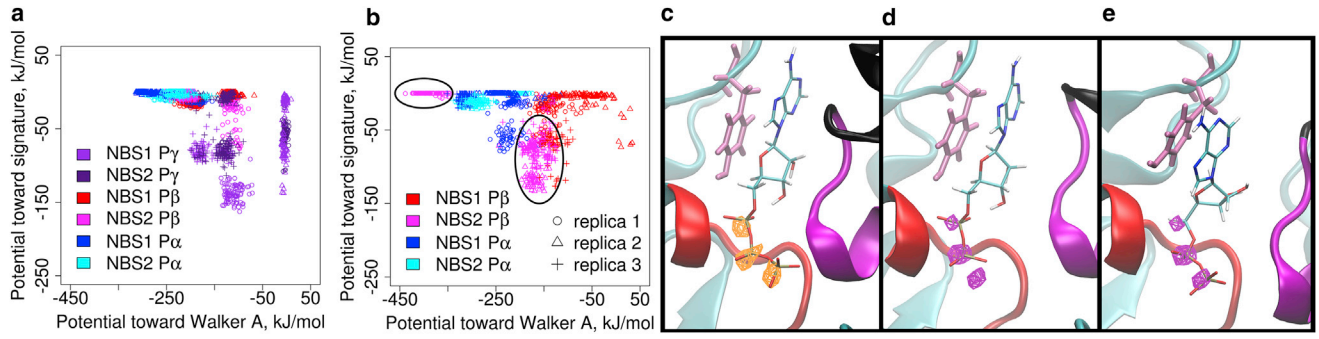

FIGURE 3 Potential energy of interaction of nucleotide phosphate groups. Energies are shown for (*a*) ATP and (*b*) ADP interacting with the Walker A and the signature motifs. Most frequent location of phosphorus atoms of (*c*) ATP (*orange*) and of (*d*) and (*e*) ADP (*purple*) is given in its two dominant conformations in unbiased simulations.

with the signature motif is similar to that of the terminal γ-phosphate (Pγ) of ATP (Pγ signature motif: ATP = −100 ± 98 kJ/mol). Both the Pβ of ADP and the Pγ of ATP carry a charge of −2 and contribute to dimerization by interacting with the signature motif. However, Pγ of ATP on average showed smaller and fluctuating interactions with the Walker A motif on the cis-NBD, whereas interactions of the terminal phosphate of ADP and the Walker A motifs were much stronger (Walker A-Pγ: ATP = −139 ± 143 kJ/mol; Pβ ADP = −334 ± 176 kJ/mol).

Fig. 3, *c–e*, shows the most likely positions of the Pα, Pβ, and Pγ atoms after fitting the trajectories to the Walker A motif. Interestingly, time averages revealed that the phosphate groups of ADP occupied the same three positions between the Walker A and the signature motif as those of ATP, highlighted by the three overlapping regions of high phosphorus occupancy. For ADP, the central area showed higher occupancy. We observed in our simulations that ADP can adopt two binding modes: in the first, the position of the Pα and Pβ overlap between ATP and ADP (Fig. 3, *c* and *d*), whereas in the second mode, ADP is shifted and its Pα and Pβ overlap with Pβ and Pγ of ATP (Fig. 3 *e*). These data indicate that the Pβ of ADP has a dual role. It interacts with the cis-NBD as the Pβ of ATP, but it also interacts with the trans-NBD as the Pγ of ATP.

Potential of mean force

Quantification of forces acting between the NBDs was carried out using PMF calculations applying the umbrella sampling technique. The starting structures for the closest distance were the same as those used for the unbiased simulations. Their initial center-of-mass distance along the probed direction (Fig. 1 *c*) was defined as zero separation. TMD1 and TMD2, which remain membrane-embedded and in contact throughout the transport cycle, restrain possible translational and rotational motions of the NBDs through the tetrahedral bundles of ICL1-4 that form stable interfaces with NBD1 and NBD2. The reaction coordinate was derived from the crystal structures by comparing the conformation of the canonical closed NBD (outward-facing) conformation with the inward facing crystal structures of the homologous mouse and *C. elegans* ABCB1 structure (PDB: 4M1M (21) and PDB: 4F4C (66), respectively). These crystal structures represent snapshots of the motion from the closed dimer (outward-facing ATP bound) to the inward-facing nucleotide-free conformation. We defined the reaction coordinate as symmetric with respect to NBS1 and NBS2 and to maximally overlap with the movements of the NBDs as observed in the crystal structure as highlighted in the Fig. S2. In every umbrella window we increased the separations of the NBDs, whereas the nucleotide and the Mg^{2+} remained bound to the core domain and the Walker A motif (Fig. 1), because nucleotides have been observed to exclusively interact with these motifs of the cis-NBD when the NBDs are separated (22,70,71).

To keep the NBDs aligned in the absence of the conformation restraining TMDs, the overall rotational degrees of freedom were removed by using enforced rotation. We could therefore increase sampling along the important degree of freedom of NBD separation. The PMF curves (Fig. 4 *a*) were calculated by the weighted histogram analysis method together with bootstrapping for error estimation. Zero level was set at full separation (at 1.2 nm).

The NBDs exert an attractive force toward each other even in the absence of nucleotides. However, the PMF profile is shallow, showing a broad minimum over ∼0.15 nm. The lowest energy conformation of the apo-NBD dimer indicates a slight opening of the NBDs and a very dynamic range of conformations. The presence of ATP in the NBS markedly increases the attractive forces to −41.8 ± 4.6 kJ/mol. Of note, error estimation correlates with the degree of variability in the dataset and represents a lower limit, because structural changes or correlations that take longer than the simulation time are not sampled and are therefore not observed. The most stable conformation is that of a closely associated NBD dimer. The PMF profile showed a deep minimum close to minimal NBD separation, followed by a steep rising slope reaching a transition point at a separation of ∼0.4 nm. A second shallower minimum exists at 0.5 nm NBD-NBD separation after which the PMF profile converged to zero at 0.8 nm. The PMF profile of the ADP-bound NBD dimer revealed a shape similar to that of ATP, with the global and the secondary minimum at the same separation. The global minimum was not as deep (−29.6 ± 3.6 kJ/mol), whereas the transition state at 0.35 nm NBD separation was of higher energy, indicative of the existence of a kinetic barrier for ADP-induced dimerization, in line with the experimental data showing that ADP cannot stabilize the same conformation of ABCB1 as ATP (24,73–75).

The presence of the transition state at 0.35 nm for ADP and 0.40 nm for the ATP configuration, which was absent in the apo configuration, suggested the existence of additional forces in the presence of nucleotides. Overall attractive and repulsive forces equal out at the transition point, thereby highlighting that both the attractive and the repulsive forces act simultaneously in the nucleotide-bound dimer.

The total potential interaction energy (Fig. 4 *b*) between the NBDs showed a monotonic distance dependence and the interaction potentials are always attractive. The potential energy profiles of ADP and ATP were similar, whereas the apo configuration showed a weaker attraction. Therefore, nucleotides make a significant contribution to the total attractive force. The curves of ADP and ATP overlapped with each other within error margins, indicating that the presence of the additional Pγ of ATP makes only a small contribution to the total enthalpic interaction energy.

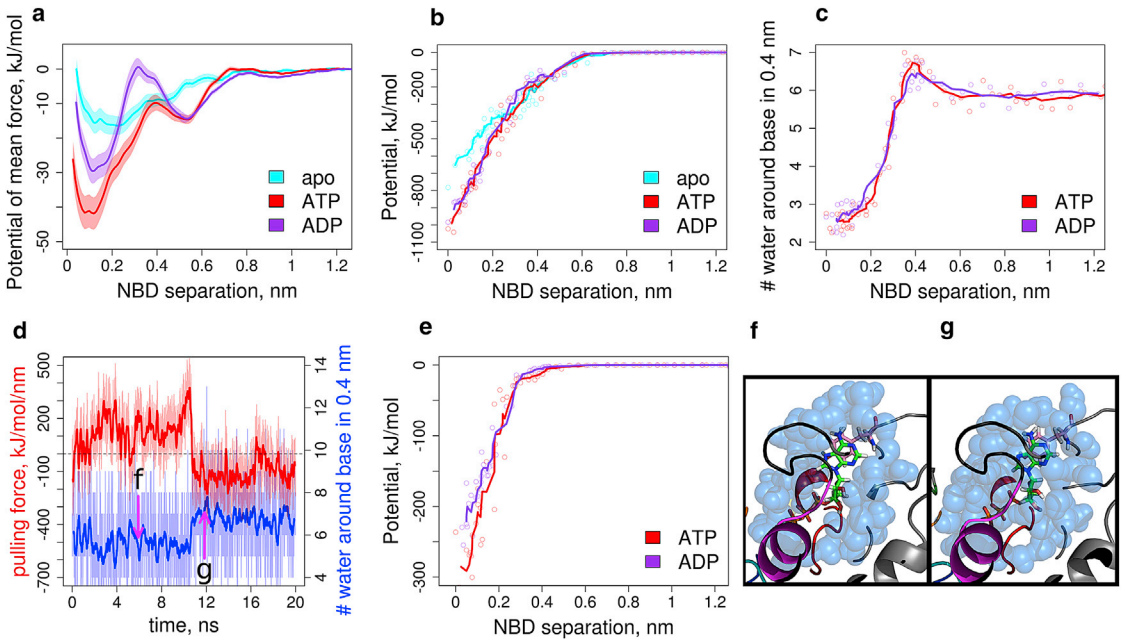

FIGURE 4 Impact of NBD separation. (*a*) PMF profile with error estimates is shown along the reaction coordinate of NBD separation. (*b*) Mean potential energy (electrostatic and van der Waals) between NBDs includes nucleotides of each umbrella window. Colored circles show actual datapoints, whereas solid lines represent smoothed curves (averaging four datapoints) to enhance clarity. (*c*) Shown here is the NBD separation dependence of the average number of water molecules around the adenine base of the nucleotide within a 0.4-nm radius. (*d*) Shown here is the pulling force in the umbrella window at 0.4 nm separation of the ATP-containing configuration (*red*). The number of water molecules around the base of ATP is shown in blue. (*e*) Given here is the mean potential interaction energy (electrostatic and van der Waals) of the phosphates with the trans-NBD. (*f–g*) Shown here is an NBS1 closeup of representative conformations for high and low water presence between the adenine base and the X-loop, viewed from the X-loop (*black*, *in front*) toward the nucleotide. (*f*) Here we show the dewetted interface; (*g*) here we show the water-filled interface. Conformations are extracted as indicated in (*d*).

Importantly, in addition to the interactions of the phosphates with both NBDs, a second strong force that kept the dimer associated arose from hydrophobic interactions between the adenine group and a hydrophobic pocket at the X-loop. These interactions were already visible in the unbiased simulations as the nucleotide base was most of the time bound to the A-loop and to the X-loop. The transition state between the two minima of the PMF profile concurred with the rapid increase in the number of water molecules between the adenine ring and the X-loop (Fig. 4 *c*). We also observed a slight peak in the number of interfacial water molecules at the separation of the transition state. Such increased density is typical for water confined between hydrophobic surfaces (76). It is caused by forcing water molecules to assume a more regular relative orientation (77) to maximize the number of hydrogen bonds. The effect therefore diminished at larger NBD separation. In the closed dimer the adenine base is in direct contact with the hydrophobic patch in the X-loop (NBD1: residues 524, 530, and 531; NBD2: residues 1169, 1175, and 1176). At initial NBD separation, these touching surfaces do not separate enough to create the required space for water molecules to enter, therefore creating a vacuum-like effect, which exerts a strong attractive force opposing NBD separation in the presence of a nucleotide. With increasing distance between 0.3 and 0.4 nm, the space became large enough to allow water molecules to enter between the hydrophobic surfaces. Water molecules confined between hydrophobic surfaces are of high energy and attract further water molecules, thereby creating a repulsive force that pushes the NBDs apart. One umbrella window at the transition point showed both counteracting forces, as water molecules moved into and out of the interface (Fig. 4, *d*, *f*, and *g*). The forces acting between the NBDs therefore changed between attractive and repulsive in response to the number of water molecules. This property of water was therefore the cause of the transition state observed between the two minima of the two nucleotide (ADP and ATP)- containing configurations and also explains the lack of a comparable maximum in the apo configuration.

The reaction coordinate of the PMF calculations was derived from conformations and movements observed in crystal structures, which impose restraints on possible motions. To test whether the reaction coordinate was not a high energy path, which could have been masked by the enforced rotation restraints that prevented rotational and translational movements of the two NBD relative to each other, we extended every umbrella window simulation by 1 ns. We thereby removed all restraints except one that maintained the probed NBD-NBD separation, which is needed because of the steep gradient along the reaction coordinate. One NBD was set to move freely except for the

distance restraint, whereas the second NBD was restrained in space. This setting was selected to circumvent the technical incompatibility of the overall tumbling of the NBD dimer with the directionality of the distance restraint, which does not follow the tumbling. Possible high energy conformation can still be unmasked, because the NBD, which is free to move, would deviate systematically from the selected path. The second NBD did not largely show any systematic translational (Fig. 5, *a–c*) or rotational (Fig. 5, *d–f*) drifts of the NBD-NBD alignment, supporting the selection of the reaction coordinate. The changes are representative of free diffusion that leads to random directional and rotational movements, although limited by direct NBD-NBD contacts. The apo system showed, as expected, the smallest deviation from the starting structures. The nucleotides did not increase much the degree of rotation compared to the apo state, and the increase was randomly distributed. Larger translational motions along the z axis (normal to the membrane plane) were detected in the ADP- and ATP-bound systems as compared to apo, but this motion would be efficiently prevented by the TMD in the full transporter setting, indicating that the applied restraints mimic the effect of the TMDs on NBD motions. Only at a separation between 0.35 and 0.45 nm might a systematic tendency of translation be present along the y direction, which was due to the hydrophobic interaction between the adenine base and the X-loop. This small shift allowed for their reattachment, while maintaining the NBD-NBD separation, because the ring system of the base is aligned at ~45 relative to the reaction coordinate of NBD separation (see Fig. 1 *b*). This motion misaligned the signature sequence with the Walker A motif and the phosphates of the nucleotides, but might be prevented by the TMDs in the full-length transporter. These data therefore show that the reaction coordinate is reasonable and the enforced rotation module limits motions that would also not be allowed in the full transporter.

Bridging waters in the interface

Water molecules in the NBD-NBD interface formed interaction networks and hydrogen-bond bridges between sides. Water density analysis (Fig. 6, *a–c*) showed that multiple water molecules are stably bound to ATP (and also to ADP). These water molecules formed, at the same time, hydrogen bonds with the trans-NBD (Fig. 6 *d*). At a separation of 0.42–0.52 nm (transition state and secondary minima on the PMF curve), stable water molecules were present between the X-loop and the adenosine (Fig. 6, *a* and *b*). However, the number of hydrogen bonds in the interface remained stable at these separations (Fig. 6 *e*). As the distance increased beyond two-to-three layers of waters molecules, the hydrogen bonding network became unstable and the number of hydrogen bonds decreased despite the increase of the total number of water molecules between the NBDs. At 0.8 nm NBD separation, the NBD-NBD interface was filled with freely moving water molecules, whereas the water density (Fig. 6 *c*) and the number of hydrogen bonds (Fig. 6 *e*) dropped to average bulk water density and dynamics—therefore no longer exerting any significant force between the NBDs.

DISCUSSION

The NBSs convert the chemical energy stored in the phosphate bonds of ATP into conformational changes of the NBDs that lead to overall structural changes of ABCB1. Our aim was to quantify the energy produced by nucleotide-induced NBD association, which can thereby be

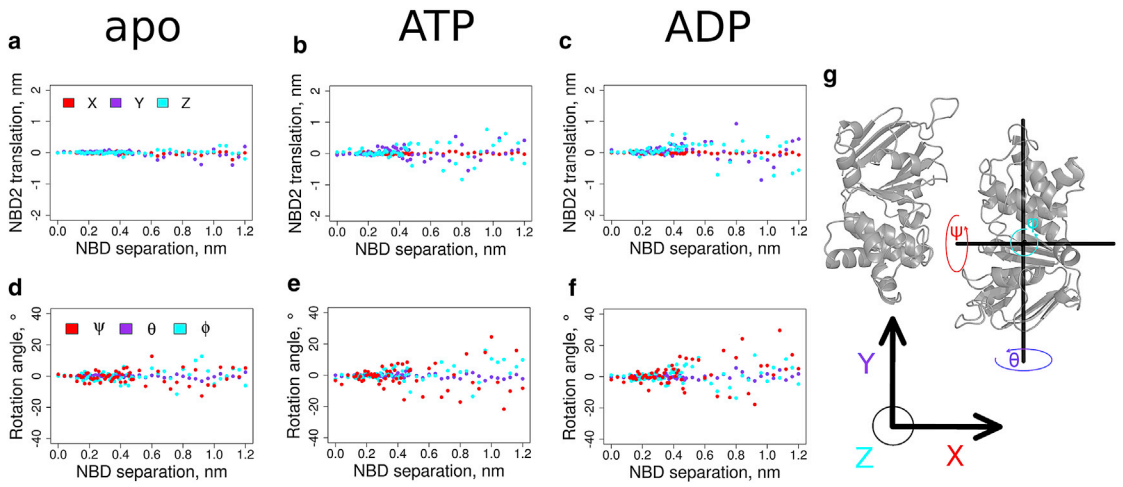

FIGURE 5 Accuracy of the reaction coordinate of the PMF calculations. Each umbrella window of the PMF calculation was extended by 1 ns without applying enforced rotation. (*a–c*) These panels show the translational movements of NBD2 relative to NBD1. The distance restraint maintaining the NBD separation is active, which leads to minimal movement in the x direction. (*d–f*) These panels show the rotation of NBD2 relative to NBD1. The direction of rotation is random and similar amplitudes are visible for the apo-, ATP-, and ADP-containing system, suggesting the absence of a masked rotational component. (*g*) Here we visualize the probed translational and rotational axes.

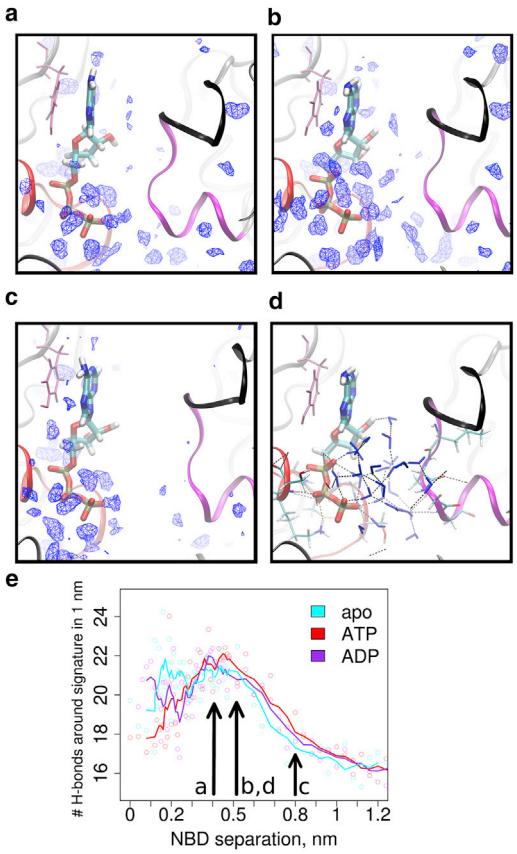

FIGURE 6 Density of water in the NBS shown (*a*) at the transition point (0.42 nm NBD separation), (*b*) at the secondary minima (0.52 nm NBD separation), and (*c*) at the noninteracting distances (0.8 nm NBD separation). The blue wireframe encloses water densities 1.5-fold higher than bulk water, therefore highlighting stably bound water molecules. (*d*) Shown here is the hydrogen-bond network between the Walker A (*red ribbon*) and signature motif (*magenta ribbon*) at the secondary minima (0.52 nm NBD separation). The X-loop is highlighted in black. (*e*) Number of hydrogen bonds within a 1 nm sphere around the signature motif, indicating the increased number of hydrogen bonds formed by the stabile bound interfacial water at small NBD separation (*colored circles* show actual datapoints, whereas *solid lines* represent a smoothed curve averaging two datapoints).

harvested by ABCB1 for directional substrate transport. We therefore created a homology model of the isolated NBDs of ABCB1 to limit the energetic consideration to the motor domains before energy transduction to the TMDs occurs. We compared the energies of NBD association for the apo-, ADP-, and ATP-bound states, and identified the underlying forces and interactions that guide NBD dimerization. Although the difference between ATP and ADP is only one phosphate group, we observed striking differences in the interactions of the phosphates with the signature motif of the trans-NBD. We found that the stability of the NBD dimer depended on the type of nucleotide bound to the NBSs. Even in the absence of any nucleotides, the apo NBDs show an inherent tendency to form dimers, stabilized by weak interactions. The PMF profile of the apo dimer revealed a broad and shallow minimum, indicative of a large ensemble of possible relative arrangements. Therefore, no specific conformation was stabilized. Unbiased simulations revealed a large range of fluctuating interdomain distances, comparable to the range of distances measured for ABCB1 by electron paramagnetic resonance (23). We find extensive opening in one NBS, but the NBD dimer never separated completely. Experimental evidence for the stability of isolated NBD dimers has been reported (78) and it has also been shown that large NBD separation is not necessary for transport as ABCB1 was able to proceed through the transport cycle while the NBDs were held together by a cross-link (29).

Nucleotides stabilized the dimer and also confined its geometry. Importantly, the interaction network of ATP and ADP within the NBS was found to be significantly different. ATP showed a well-defined binding geometry with a dimerization energy of -41.8 ± 4.6 kJ/mol. The ATP-bound dimer was stable and largely symmetric in unbiased simulations and showed a narrow conformational ensemble. In these conformations, ATP is tightly bound to motifs of the cis-NBD, whereas Pγ reached out and strongly interacted with the signature motif of the trans-NBD. ADP also showed a sharp energy minimum of -29.6 ± 3.6 kJ/mol, but the two phosphate atoms of ADP failed to simultaneously maintain all interaction networks provided by ATP. In particular, the lack of Pγ prevents ADP from simultaneously maintaining connections encompassing 1) Walker A–nucleotide–signature motif and 2) Walker A–nucleotide–Mg^{2+}–Walker B and Q-loop. Instead, ADP shifted the position of its two phosphate groups, thereby altering the interaction network between them from forming strong interactions with the signature motif on the trans-NBD or with the Walker B and Q-loop on the cis-NBD. The network of interactions in the NBS of the ADP bound state excludes strong interactions with the trans-NBD in one of the two conformations, thereby reducing the stability of the complex and the close association of the NBD dimer. Unbiased simulations confirmed this weakened interaction network that stabilizes the closed NBS geometry. The ADP-bound systems showed partial asymmetric opening of the NBS, in which the Pβ of ADP did not directly interact with the signature motif. The overall shape of the PMF profile and the associated energies indicated that the presence of ADP alone would not promote NBD separation, but also that reaching the canonical dimer conformation is inhibited by a large kinetic barrier that separates the open from the closed conformation. The barrier was much smaller (comparable to kT) for ATP, consistent with the observation that ATP or nonhydrolyzable ATP analogs can reach the nucleotide occluded conformation, whereas ADP is not able to promote or stabilize the same conformation (24,73–75). ADP therefore does not support transport, but it was experimentally found that the binding affinity of ADP is comparable that of ATP (K_D(ATP) = 0.28 mM;

K_D(ADP) = 0.33 mM) (79) consistent with the deep primary minimum. Also, Sav1866 was crystallized in an outward open conformation with two bound AMP-PNP or ADP molecules (6), supporting the notion that ADP can stabilize the NBD dimer. The existence of a kinetic barrier is therefore essential, because the intracellular concentration of ADP is comparable to its K_D; ADP would therefore be an effective inhibitor for ABCB1 transporter function, if not prevented from binding.

In this study we identified an underappreciated role of water molecules, which play key roles in 1) connecting the NBDs at medium separation via a hydrogen bonding network and 2) mediating important interactions between the X/A loops and the adenine base through the hydrophobic effect. Interactions of the nucleotide with the A-loop were found in nucleotide-bound crystal structures and also have been verified experimentally (3). Mutations of either the A-loop (80) or the X-loop (81) sequences showed strong effects on ATP hydrolysis and transport. The PMF profiles of ATP and ADP revealed an unpredicted high energy transition point separating two energy minima. Fig. 4 shows that hydrophobic interactions of the adenine base are responsible for the observed effect. We found that both the A-loop and the X-loop formed hydrophobic interactions with the adenine base, thus stabilizing a nucleotide sandwiched conformation. This interaction relay provides a large energetic contribution to dimerization that locks the nucleotide-bound closed conformation and creates a barrier for NBD-NBD separation. Also shown by the PMF profile, rupture of these hydrophobic interactions requires a large force that coincides with water entering between the hydrophobic surfaces of the base and of the protein (Fig. 4 *c*). Water density was especially high at small separation, which is typical for water molecules in confined hydrophobic space (76), but also energetically unfavorable, supporting the interpretation that the hydrophobic interactions of the nucleotide base play an important role in maintaining the defined geometry of the nucleotide bound state. At a separation that is too small to allow for water to enter, work for creating the void volume is still required, which adds to the energy barrier.

Our results indicate that dimerization of separated, nucleotide-bound NBDs proceeds along a hierarchical sequence of four steps: 1) At 0.6 nm, a water-bridged network forms between NBDs and the interaction potential becomes attractive. 2) At 0.5 nm distance, water becomes confined between the hydrophobic interface of the X-loop and the adenine base, which creates a barrier to further distance reduction. 3) At 0.35 nm separation, the interface between the X-loop and the adenine base is dewetting, creating a strong force toward further association that leads to a sharp drop in the PMF profile. 4) At distances <0.3 nm, the γP of ATP forms coordinated interactions with the signature motif, ensuring that a proper dimer is formed.

The pattern of interaction among the NBDs, the nucleotide, and the Mg^{2+} ion differ strongly among the apo-, ADP-, and ATP-bound states. The interaction graph of the apo dimer showed the lowest number of interactions between motifs within the monomer and across the dimer interface. ADP only slightly increased the number of interactions. In contrast, in the presence of ATP, a large number of inter- and intradomain interactions were found. Most interactions across the dimer interface-connected motifs through contributions of ATP. These data show that binding of ATP can, through enhanced motif interactions, generate forces that lock the NBDs into a specific conformation. These interactions represent an input of energy into the NBDs, the motor domain of ABCB1, and might be associated with a power stroke of the transport cycle.

It has been shown experimentally that ATP occlusion occurs before hydrolysis in only one NBS. In wild-type ABCB1, one molecule of the nonhydrolyzable ATP analog ATPγS was bound. Similarly, one ATP molecule was trapped in the catalytic glutamate mutant (E556Q/E1201Q) per transporter (82–84). This ratio of one nucleotide per transporter was interpreted as being indicative of an asymmetric occlusion of one nucleotide. Asymmetry in NBS geometry was also observed in simulations (20,38–41). Recent experiments with mouse ABCB1 with a shortened linker region showed that NBS1 has higher ATPase activity (22), which is in-line with our observations of a more likely occlusion of ATP in NBS1. We selected a symmetric reaction coordinate, because crystal structures of ABCB1 (Fig. S2) indicated that NBD separation would follow a symmetric path. Also transport cycle models that include full NBD separation typically predict symmetric movements. We carried out an estimation of structural drifts for each PMF window (Fig. 5) to identify any indication that the reaction path could have been of high energy, which would lead to a systematic drift in relative NBD-NBD rotation. Rotations were randomly distributed, indicative that the isolated NBDs can associate symmetrically, if the same nucleotide is present in both NBSs. Presence of ATP in both NBSs is very likely, because the ATP concentration in the cytosol exceeds K_D by a large extent. The small systematic drift at intermediate separation indicates the possibility of a noncomplete symmetric geometry, but the experimentally observed asymmetry could be contingent to the presence of the TMDs. Importantly, the PMF profiles showed two minima in the nucleotide-bound state. Our data might therefore suggest that in an asymmetric conformation one NBS resides in the first minimum, whereas the second NBS assumes the geometry of the secondary minimum, thereby predisposing for ADP release after hydrolysis.

CONCLUSIONS

ATP consumption by the NBDs energizes the transport cycle of ABCB1 by inducing conformational changes that

are transmitted from the NBDs or motor domains to the TMDs, which recognize and translocate substrate. We use computational methods to quantify the energy input by ATP that leads to NBD dimerization. A comparison with the apo and the posthydrolytic ADP revealed that ATP stabilizes the NBD dimer in a well-defined conformation, acting as glue through specific hydrogen bonds and electrostatic and hydrophobic interactions. This strongly interconnected ATP bound dimer is rigid and can therefore efficiently propagate forces toward the TMDs, representing a power stroke of the transport cycle by ABCB1. The structure-stabilizing network is disrupted in the posthydrolytic ADP-bound state and largely absent in the apo state, leading to structural rearrangement in the NBDs and consequently to the TMDs.

SUPPORTING MATERIAL

Supporting Materials and Methods and nine figures are available at http://www.biophysj.org/biophysj/supplemental/S0006-3495(17)31254-7.

AUTHOR CONTRIBUTIONS

D.S. performed the simulations, analyzed the data, and took part in writing the manuscript. G.S. and P.C. took part in writing the manuscript. T.S. designed the research and wrote the article.

ACKNOWLEDGMENTS

We thankfully acknowledge the financial support by the Austrian Science Fund, project F3509 to P.C., F3524 to T.S., and F3525 to G.S., and EU-sponsored COST Action CM1306 to T.S. We are grateful for computing time allocated by the Vienna Scientific Cluster (VSC) to T.S.

REFERENCES

1. Chen, C. J., J. E. Chin, …, I. B. Roninson. 1986. Internal duplication and homology with bacterial transport proteins in the mdr1 (P-glycoprotein) gene from multidrug-resistant human cells. *Cell.* 47:381–389.
2. Raviv, Y., H. B. Pollard, …, M. M. Gottesman. 1990. Photosensitized labeling of a functional multidrug transporter in living drug-resistant tumor cells. *J. Biol. Chem.* 265:3975–3980.
3. Ambudkar, S. V., I. W. Kim, …, Z. E. Sauna. 2006. The A-loop, a novel conserved aromatic acid subdomain upstream of the Walker A motif in ABC transporters, is critical for ATP binding. *FEBS Lett.* 580:1049–1055.
4. Walker, J. E., M. Saraste, …, N. J. Gay. 1982. Distantly related sequences in the α- and β-subunits of ATP synthase, myosin, kinases and other ATP-requiring enzymes and a common nucleotide binding fold. *EMBO J.* 1:945–951.
5. Ambudkar, S. V., I. W. Kim, and Z. E. Sauna. 2006. The power of the pump: mechanisms of action of P-glycoprotein (ABCB1). *Eur. J. Pharm. Sci.* 27:392–400.
6. Dawson, R. J., and K. P. Locher. 2006. Structure of a bacterial multidrug ABC transporter. *Nature.* 443:180–185.
7. Higgins, C. F. 1992. ABC transporters: from microorganisms to man. *Annu. Rev. Cell Biol.* 8:67–113.
8. Geourjon, C., C. Orelle, …, J. M. Jault. 2001. A common mechanism for ATP hydrolysis in ABC transporter and helicase superfamilies. *Trends Biochem. Sci.* 26:539–544.
9. Schneider, E., and S. Hunke. 1998. ATP-binding-cassette (ABC) transport systems: functional and structural aspects of the ATP-hydrolyzing subunits/domains. *FEMS Microbiol. Rev.* 22:1–20.
10. Zaitseva, J., S. Jenewein, …, L. Schmitt. 2005. H662 is the linchpin of ATP hydrolysis in the nucleotide-binding domain of the ABC transporter HlyB. *EMBO J.* 24:1901–1910.
11. Jardetzky, O. 1966. Simple allosteric model for membrane pumps. *Nature.* 211:969–970.
12. Rees, D. C., E. Johnson, and O. Lewinson. 2009. ABC transporters: the power to change. *Nat. Rev. Mol. Cell Biol.* 10:218–227.
13. Davidson, A. L., S. S. Laghaeian, and D. E. Mannering. 1996. The maltose transport system of *Escherichia coli* displays positive cooperativity in ATP hydrolysis. *J. Biol. Chem.* 271:4858–4863.
14. Sauna, Z. E., and S. V. Ambudkar. 2001. Characterization of the catalytic cycle of ATP hydrolysis by human P-glycoprotein. The two ATP hydrolysis events in a single catalytic cycle are kinetically similar but affect different functional outcomes. *J. Biol. Chem.* 276:11653–11661.
15. Sauna, Z. E., and S. V. Ambudkar. 2007. About a switch: how P-glycoprotein (ABCB1) harnesses the energy of ATP binding and hydrolysis to do mechanical work. *Mol. Cancer Ther.* 6:13–23.
16. Loo, T. W., and D. M. Clarke. 1997. Drug-stimulated ATPase activity of human P-glycoprotein requires movement between transmembrane segments 6 and 12. *J. Biol. Chem.* 272:20986–20989.
17. Chen, J., G. Lu, …, F. A. Quiocho. 2003. A tweezers-like motion of the ATP-binding cassette dimer in an ABC transport cycle. *Mol. Cell.* 12:651–661.
18. Higgins, C. F., and K. J. Linton. 2004. The ATP switch model for ABC transporters. *Nat. Struct. Mol. Biol.* 11:918–926.
19. van der Does, C., and R. Tampé. 2004. How do ABC transporters drive transport? *Biol. Chem.* 385:927–933.
20. Jones, P. M., and A. M. George. 2009. Opening of the ADP-bound active site in the ABC transporter ATPase dimer: evidence for a constant contact, alternating sites model for the catalytic cycle. *Proteins.* 75:387–396.
21. Li, J., K. F. Jaimes, and S. G. Aller. 2014. Refined structures of mouse P-glycoprotein. *Protein Sci.* 23:34–46.
22. Esser, L., F. Zhou, …, D. Xia. 2017. Structures of the multidrug transporter P-glycoprotein reveal asymmetric ATP binding and the mechanism of polyspecificity. *J. Biol. Chem.* 292:446–461.
23. Wen, P. C., B. Verhalen, …, E. Tajkhorshid. 2013. On the origin of large flexibility of P-glycoprotein in the inward-facing state. *J. Biol. Chem.* 288:19211–19220.
24. Verhalen, B., R. Dastvan, …, H. S. Mchaourab. 2017. Energy transduction and alternating access of the mammalian ABC transporter P-glycoprotein. *Nature.* 543:738–741.
25. van Wonderen, J. H., R. M. McMahon, …, R. Callaghan. 2014. The central cavity of ABCB1 undergoes alternating access during ATP hydrolysis. *FEBS J.* 281:2190–2201.
26. Verhalen, B., S. Ernst, …, S. Wilkens. 2012. Dynamic ligand-induced conformational rearrangements in P-glycoprotein as probed by fluorescence resonance energy transfer spectroscopy. *J. Biol. Chem.* 287:1112–1127.
27. Qu, Q., and F. J. Sharom. 2001. FRET analysis indicates that the two ATPase active sites of the P-glycoprotein multidrug transporter are closely associated. *Biochemistry.* 40:1413–1422.
28. Zarrabi, N., S. Ernst, …, M. Börsch. 2014. Analyzing conformational dynamics of single P-glycoprotein transporters by Förster resonance energy transfer using hidden Markov models. *Methods.* 66:168–179.
29. Loo, T. W., M. C. Bartlett, …, D. M. Clarke. 2012. The ATPase activity of the P-glycoprotein drug pump is highly activated when the N-terminal and central regions of the nucleotide-binding domains are linked closely together. *J. Biol. Chem.* 287:26806–26816.
30. Loo, T. W., M. C. Bartlett, and D. M. Clarke. 2002. The "LSGGQ" motif in each nucleotide-binding domain of human P-glycoprotein is adjacent to the opposing Walker A sequence. *J. Biol. Chem.* 277:41303–41306.

31. Loo, T. W., M. C. Bartlett, and D. M. Clarke. 2003. Drug binding in human P-glycoprotein causes conformational changes in both nucleotide-binding domains. *J. Biol. Chem.* 278:1575–1578.

32. Loo, T. W., M. C. Bartlett, and D. M. Clarke. 2010. Human P-glycoprotein is active when the two halves are clamped together in the closed conformation. *Biochem. Biophys. Res. Commun.* 395:436–440.

33. Loo, T. W., and D. M. Clarke. 2000. Drug-stimulated ATPase activity of human P-glycoprotein is blocked by disulfide cross-linking between the nucleotide-binding sites. *J. Biol. Chem.* 275:19435–19438.

34. Chang, S. Y., F. F. Liu, …, Y. Sun. 2013. Molecular insight into conformational transmission of human P-glycoprotein. *J. Chem. Phys.* 139:225102.

35. Moradi, M., and E. Tajkhorshid. 2014. Computational recipe for efficient description of large-scale conformational changes in biomolecular systems. *J. Chem. Theory Comput.* 10:2866–2880.

36. Moradi, M., and E. Tajkhorshid. 2013. Mechanistic picture for conformational transition of a membrane transporter at atomic resolution. *Proc. Natl. Acad. Sci. USA.* 110:18916–18921.

37. Wise, J. G. 2012. Catalytic transitions in the human MDR1 P-glycoprotein drug binding sites. *Biochemistry.* 51:5125–5141.

38. George, A. M., and P. M. Jones. 2013. An asymmetric post-hydrolysis state of the ABC transporter ATPase dimer. *PLoS One.* 8:e59854.

39. Jones, P. M., and A. M. George. 2017. How intrinsic dynamics mediates the allosteric mechanism in the ABC transporter nucleotide binding domain dimer. *J. Chem. Theory Comput.* 13:1712–1722.

40. Aittoniemi, J., H. de Wet, …, M. S. Sansom. 2010. Asymmetric switching in a homodimeric ABC transporter: a simulation study. *PLOS Comput. Biol.* 6:e1000762.

41. Ma, J., and P. C. Biggin. 2013. Substrate versus inhibitor dynamics of P-glycoprotein. *Proteins.* 81:1653–1668.

42. Furuta, T., Y. Sato, and M. Sakurai. 2016. Structural dynamics of the heterodimeric ABC transporter TM287/288 induced by ATP and substrate binding. *Biochemistry.* 55:6730–6738.

43. Pan, L., and S. G. Aller. 2015. Equilibrated atomic models of outward-facing P-glycoprotein and effect of ATP binding on structural dynamics. *Sci. Rep.* 5:7880.

44. Xu, Y., A. Seelig, and S. Bernèche. 2017. Unidirectional transport mechanism in an ATP dependent exporter. *ACS Cent Sci.* 3:250–258.

45. Jones, P. M., and A. M. George. 2011. Molecular-dynamics simulations of the ATP/apo state of a multidrug ATP-binding cassette transporter provide a structural and mechanistic basis for the asymmetric occluded state. *Biophys. J.* 100:3025–3034.

46. O'Mara, M. L., and A. E. Mark. 2014. Structural characterization of two metastable ATP-bound states of P-glycoprotein. *PLoS One.* 9:e91916.

47. Wen, P. C., and E. Tajkhorshid. 2008. Dimer opening of the nucleotide binding domains of ABC transporters after ATP hydrolysis. *Biophys. J.* 95:5100–5110.

48. McCormick, J. W., P. D. Vogel, and J. G. Wise. 2015. Multiple drug transport pathways through human P-glycoprotein. *Biochemistry.* 54:4374–4390.

49. Prajapati, R., and A. T. Sangamwar. 2014. Translocation mechanism of P-glycoprotein and conformational changes occurring at drug-binding site: insights from multi-targeted molecular dynamics. *Biochim. Biophys. Acta.* 1838:2882–2898.

50. O'Mara, M. L., and A. E. Mark. 2012. The effect of environment on the structure of a membrane protein: P-glycoprotein under physiological conditions. *J. Chem. Theory Comput.* 8:3964–3976.

51. Stockner, T., S. J. de Vries, …, P. Chiba. 2009. Data-driven homology modelling of P-glycoprotein in the ATP-bound state indicates flexibility of the transmembrane domains. *FEBS J.* 276:964–972.

52. Dawson, R. J., and K. P. Locher. 2007. Structure of the multidrug ABC transporter Sav1866 from *Staphylococcus aureus* in complex with AMP-PNP. *FEBS Lett.* 581:935–938.

53. Fiser, A., and A. Sali. 2003. MODELLER: generation and refinement of homology-based protein structure models. *Methods Enzymol.* 374:461–491.

54. Shen, M. Y., and A. Sali. 2006. Statistical potential for assessment and prediction of protein structures. *Protein Sci.* 15:2507–2524.

55. Best, R. B., and G. Hummer. 2009. Optimized molecular dynamics force fields applied to the helix-coil transition of polypeptides. *J. Phys. Chem. B.* 113:9004–9015.

56. Wang, J., R. M. Wolf, …, D. A. Case. 2004. Development and testing of a general AMBER force field. *J. Comput. Chem.* 25:1157–1174.

57. Meagher, K. L., L. T. Redman, and H. A. Carlson. 2003. Development of polyphosphate parameters for use with the AMBER force field. *J. Comput. Chem.* 24:1016–1025.

58. Sousa da Silva, A. W., and W. F. Vranken. 2012. ACPYPE—ante chamber PYTHON parser interface. *BMC Res. Notes.* 5:367.

59. Abraham, M. J., T. Murtola, …, E. Lindahl. 2015. GROMACS: high performance molecular simulations through multi-level parallelism from laptops to supercomputers. *SoftwareX.* 1–2:19–25.

60. Bussi, G., D. Donadio, and M. Parrinello. 2007. Canonical sampling through velocity rescaling. *J. Chem. Phys.* 126:014101.

61. Parrinello, M., and A. Rahman. 1981. Polymorphic transitions in single crystals—a new molecular-dynamics method. *J. Appl. Phys.* 52:7182–7190.

62. Essmann, U., L. Perera, …, L. G. Pedersen. 1995. A smooth particle mesh Ewald method. *J. Chem. Phys.* 103:8577–8593.

63. Leach, A. R. 2001. Molecular Modelling: Principles and Applications. Pearson Education, White Plains, NY.

64. Hub, J. S., B. L. de Groot, and D. van der Spoel. 2010. g_WHAM—a free weighted histogram analysis implementation including robust error and autocorrelation estimates. *J. Chem. Theory Comput.* 6:3713–3720.

65. Kumar, S., D. Bouzida, …, J. M. Rosenberg. 1992. The weighted histogram analysis method for free-energy calculations on biomolecules. 1. The method. *J. Comput. Chem.* 13:1011–1021.

66. Jin, M. S., M. L. Oldham, …, J. Chen. 2012. Crystal structure of the multidrug transporter P-glycoprotein from *Caenorhabditis elegans*. *Nature.* 490:566–569.

67. Kutzner, C., J. Czub, and H. Grubmüller. 2011. Keep it flexible: driving macromolecular rotary motions in atomistic simulations with GROMACS. *J. Chem. Theory Comput.* 7:1381–1393.

68. Hung, L. W., I. X. Wang, …, S. H. Kim. 1998. Crystal structure of the ATP-binding subunit of an ABC transporter. *Nature.* 396:703–707.

69. Oldham, M. L., and J. Chen. 2011. Crystal structure of the maltose transporter in a pretranslocation intermediate state. *Science.* 332:1202–1205.

70. Ramaen, O., S. Masscheleyn, …, E. Jacquet. 2003. Biochemical characterization and NMR studies of the nucleotide-binding domain 1 of multidrug-resistance-associated protein 1: evidence for interaction between ATP and Trp^{653}. *Biochem. J.* 376:749–756.

71. Shintre, C. A., A. C. Pike, …, E. P. Carpenter. 2013. Structures of ABCB10, a human ATP-binding cassette transporter in apo- and nucleotide-bound states. *Proc. Natl. Acad. Sci. USA.* 110:9710–9715.

72. Gumbart, J. C., B. Roux, and C. Chipot. 2013. Efficient determination of protein-protein standard binding free energies from first principles. *J. Chem. Theory Comput.* 9. https://doi.org/10.1021/ct400273t.

73. Bársony, O., G. Szalóki, …, K. Goda. 2016. A single active catalytic site is sufficient to promote transport in P-glycoprotein. *Sci. Rep.* 6:24810.

74. Lu, G., J. M. Westbrooks, …, J. Chen. 2005. ATP hydrolysis is required to reset the ATP-binding cassette dimer into the resting-state conformation. *Proc. Natl. Acad. Sci. USA.* 102:17969–17974.

75. Moody, J. E., L. Millen, …, P. J. Thomas. 2002. Cooperative, ATP-dependent association of the nucleotide binding cassettes during the catalytic cycle of ATP-binding cassette transporters. *J. Biol. Chem.* 277:21111–21114.

76. Kanduč, M., A. Schlaich, …, R. R. Netz. 2016. Water-mediated interactions between hydrophilic and hydrophobic surfaces. *Langmuir.* 32:8767–8782.

77. Bianco, V., and G. Franzese. 2014. Critical behavior of a water monolayer under hydrophobic confinement. *Sci. Rep.* 4:4440.

78. Pretz, M. G., S. V. Albers, …, C. van der Does. 2006. Thermodynamics of the ATPase cycle of GlcV, the nucleotide-binding domain of the glucose ABC transporter of *Sulfolobus solfataricus*. *Biochemistry.* 45:15056–15067.

79. Siarheyeva, A., R. Liu, and F. J. Sharom. 2010. Characterization of an asymmetric occluded state of P-glycoprotein with two bound nucleotides: implications for catalysis. *J. Biol. Chem.* 285:7575–7586.

80. Carrier, I., I. L. Urbatsch, …, P. Gros. 2007. Mutational analysis of conserved aromatic residues in the A-loop of the ABC transporter ABCB1A (mouse Mdr3). *FEBS Lett.* 581:301–308.

81. Kluth, M., J. Stindt, …, L. Schmitt. 2015. A mutation within the extended X loop abolished substrate-induced ATPase activity of the human liver ATP-binding cassette (ABC) transporter MDR3. *J. Biol. Chem.* 290:4896–4907.

82. Oloo, E. O., and D. P. Tieleman. 2004. Conformational transitions induced by the binding of MgATP to the vitamin B12 ATP-binding cassette (ABC) transporter BtuCD. *J. Biol. Chem.* 279:45013–45019.

83. Sauna, Z. E., I. W. Kim, …, S. V. Ambudkar. 2007. Catalytic cycle of ATP hydrolysis by P-glycoprotein: evidence for formation of the E.S reaction intermediate with ATP-γ-S, a nonhydrolyzable analogue of ATP. *Biochemistry.* 46:13787–13799.

84. Tombline, G., and A. E. Senior. 2005. The occluded nucleotide conformation of P-glycoprotein. *J. Bioenerg. Biomembr.* 37:497–500.